JOURNAL OF SPACECRAFT AND ROCKETS
Vol. 59, No. 4, July–August 2022

Formation of Bow Shock Waves Around a Blunt Body in Magnetohydrodynamics Flows

Yixiang Li,* Qiu Wang,† Kai Luo,‡ and Wei Zhao§
Chinese Academy of Sciences, 100190 Beijing, People's Republic of China

https://doi.org/10.2514/1.A35315

The diffraction of a shock wave over a stationary body is a problem of interest associated with the starting of shock tubes and expansion tubes, which are well suited to studies of hypersonic magnetohydrodynamic flows. However, these facilities are characterized by very short test times. The transient parameters during the establishment of the detached bow shock in such impulsive facilities are important for both data processing and experimental design. In the present study, based on the low magnetic Reynolds number assumption and dipole magnetic field distribution, the influence of magnetic field on the diffraction of an incident shock wave over a sphere was studied numerically. The incident shock Mach number ranges from 11 to 15 under different magnetic field intensities. Time histories of the shock-detached distance and stagnation pressure were first obtained. Moreover, the time needed to establish the steady flows over the sphere was also displaced against the magnetic interaction parameter. The larger the magnetic interaction parameter, the longer the time needed to establish a steady bow shock for experiments, which further challenges the facilities to have sufficient test times for conducting hypersonic magnetohydrodynamic flow experiments.

I. Introduction

IN RECENT decades, a renewed interest has grown in hypersonic flight. In the design of hypersonic vehicles, aerodynamic heating is one of the primary issues that needs to be carefully dealt with, because enormous challenges are posed with the survival of hypersonic flight due to the severe heating, such as high heat flux at stagnation point and significant increase in heat transfer by laminar–turbulent transition, etc. Therefore, various thermal protection methods have been developed by researchers to protect the vehicles from severe aerodynamic heating. As effective ways of thermal protection, flow control technologies have been widely investigated, including boundary-layer transition control [1–3], shock spike technology [4], opposing jet technology [5], and so forth. Among these methods, magnetohydrodynamic (MHD) flow control, an earlier-proposed active and noninvasive thermal protection technique, has attracted intense interest due to the recent improvements in electromagnet technology and superconducting materials. In hypersonic MHD flow control, a magnetic field is applied to a weakly ionized plasma flow in the shock layer ahead of a hypersonic flight vehicle. The interaction between the magnetic field and the plasma flow induces the Lorentz force. The plasma flow is decelerated by the Lorentz force, which leads to the enlargement of the shock layer. As a result, the tangential velocity gradient near the stagnation point is reduced, which leads to a smaller convective heat flux [6]. Additionally, MHD flow control also has broad application prospects in radio-blackout mitigation [7,8], air-breathing engine augmentation [9], flight control [10–12], and MHD power generation [9].

In the earliest stage of research on MHD flow control, researchers mainly conducted theoretical analysis on simple models, such as flat plate and sphere [13–16]. For example, Bush investigated the influence of magnetic field on the flow of conductive fluids in the shock layer [17]. Later, the feasibility of applying magnetic technology to hypersonic vehicles and their propulsion systems was proved through theory [18,19], experiments [20–25], and numerical simulations [26–28]. However, due to the complexity of MHD technology, its research is still in the exploratory research stage, and there are still a lot of fundamental issues that need to be addressed. Experimental methods are critical for the development of MHD flow control. Due to the high enthalpy required to ensure the test flow has an adequate conductivity, only certain facilities worldwide can facilitate these experiments. For these high-enthalpy facilities, the higher total temperature conditions are always achieved at the expense of the test time, leading to very short effective test times. Also, generally, the higher the enthalpy is, the shorter the test time is. For example, the test time of the High Enthalpy Shock Tunnel Göttingen, a reflected shock tunnel facility at Göttingen University, is 1–6 ms [29], and that of the X2 expansion tunnel at the University of Queensland is 50–200 μs [30]. In addition, the test time of the Φ800 shock tube at the Institute of Mechanics, Chinese Academy of Sciences is only tens of microseconds [31]. Therefore, there is always a question as to whether or not the test times are sufficient to allow the establishment of certain types of steady flows over aerodynamic models. If available test times are not sufficiently long to obtain a steady-state flow over aerodynamic models, the experimental data of these facilities are not reliable for an accurate representation of simulated flowfields.

In hypersonic MHD flows, the electromagnetic force is generated by the interaction between the magnetic field and the conductive fluid according to Faraday's law of induction. This force has a component in the direction opposite to the freestream velocity vector and pushes the shock away from the body. Thus, diffraction of the shock around the model and the time needed to establish the bow shock will be affected. Lefevre et al. [32] performed experimental observation of hypersonic MHD shock-detached distance in the X2 expansion tunnel, with air as the test gas, and a flow velocity of up to 12–14 km/s. The test time was about 100 μs. He clearly observed the unsteady change of shock-detached distance within the effective test time range of 20–80 μs. However, the reason for the unsteady change was not explained in detail. For the flow without magnetic field, Patz [33] studied the time history of the bow shock formation from a theoretical perspective and compared it with the shock- tube experiments. Moran and Moorhem [34] and Barnwell [35] used a numerical simulation method to calculate the flowfield after the arrival of the incident shock, and predicted the pressure distribution on the smooth blunt body in a

Received 28 November 2021; revision received 17 February 2022; accepted for publication 18 February 2022; published online 23 March 2022.

*Master's Student, State Key Laboratory of High Temperature Gas Dynamics, Institute of Mechanics.

†Associate Professor, State Key Laboratory of High Temperature Gas Dynamics, Institute of Mechanics; wangqiu@imech.ac.cn (Corresponding Author).

‡Ph.D. Student, State Key Laboratory of High Temperature Gas Dynamics, Institute of Mechanics.

§Professor, State Key Laboratory of High Temperature Gas Dynamics, Institute of Mechanics.

relatively long test time. Miller and Moore [36] reported that the time required for heat flux at the stagnation point to reach basic stability is about 80 μs. However, the formation of the bow shock waves around the blunt bodies in the MHD flow has not yet been reported, which deserves more attention due to the extreme test condition and the influence of the magnetic field on the flowfield establishment.

In view of the importance of the time needed for establishment of the detached bow shock in MHD flows, the primary goal of the present study was to examine the influence of magnetic field on its detach shock movement. The axisymmetric two-dimensional thermochemical nonequilibrium MHD numerical simulations were conducted under different magnetic field intensities. Different incident shock Mach numbers was considered. The unsteady flow processes were examined in detail to provide theoretical guidance for both data processing and experimental design of hypersonic MHD flow control experiments.

II. Physical Problem

In the present study, the influence of magnetic field on the motion of the bow shock out from a sphere in an unsteady process is studied. Diffraction of an incident shock wave over a sphere is illustrated in Fig. 1. A strong shock moving in a gas at rest and sweeping over a sphere is reflected at the stagnation point. The reflected shock running upstream is decelerated and, after a specific formation time, establishes as a steady bow shock wave at the distance Δ from the stagnation point, where Δ represents the steady bow shock standoff distance. To identify flow regions defined by the incident and reflected shock waves and the wall, numbers are used as shown in Fig. 1. Region ① represents the undisturbed flow in front of the incident shock, region ② represents the properties behind the incident shock, and region ③ represents the properties between the reflected shock and the wall. Phenomena that are treated include the diffraction of the incident shock wave by the sphere and the unsteady flow in the shock layer ahead of the body after shock impingement and before the establishment of steady flow.

For the preceding physical process with the existence of an applied magnetic field, additional Lorentz force will be introduced due to the interaction between the magnetic field and the charged particles in the shock layer. Certainly, the shock should be strong enough to create ionization of the gas in the shock layer. Then, the Lorentz force will increase the final shock standoff distance, as illustrated in Fig. 2. However, the present study mainly focuses on the unsteady bow shock formation process after applying a magnetic field; this is quite important for the MHD experiments in shock tube or expansion tube, where the test time is extremely short.

Several dimensionless parameters have been shown to be of importance when determining the magnitude of the MHD effect. The magnetic interaction parameter is the most important, which describes the relative magnitude between electromagnetic forces and inertial flow forces:

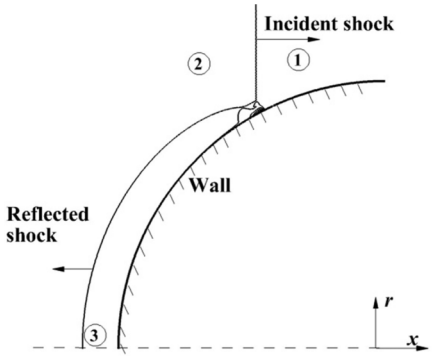

Fig. 1 Shock reflection at a sphere; numbers are used to identify flow regions defined by the incident and reflected shock waves and the wall.

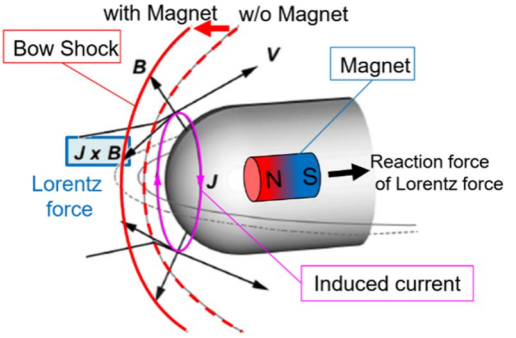

Fig. 2 Flow around reentry vehicle with an applied magnetic field and the resulting Lorentz force. *J*, *B*, and *V* are, respectively, vectors of electric current, magnetic field, and flow velocity [37] (Reprinted in part with permission from Nagata, Y., Satofukay, Y., Watanabey, Y., Tezukaz, A., Yamadax, K., and Abe, T., "Experimental Study on the Magneto-aerodynamic Force Deflected by Magnetic Field Interaction in a Weakly-ionized Plasma Flow," AIAA Paper 2013-2999, January 2013. Copyright 2013 by the American Institute of Aeronautics and Astronautics, Inc.).

$$Q = \frac{\sigma B_0^2 L}{\rho_\infty u_\infty} \tag{1}$$

where σ is the electrical conductivity, B_0 is the characteristic magnetic field flux density at the stagnation point in this study, L is the characteristic length or sphere radius in the present study, ρ_∞ is freestream density, and u_∞ is the freestream velocity. Generally, MHD effects should become significant for $Q > 1$ [32].

Another important dimensionless parameter is the magnetic Reynolds number. It gives an estimate to the extent to which the magnetic field deforms due to the presence of plasma:

$$Re_m = \sigma u_\infty L \mu_0 \tag{2}$$

where μ_0 is the magnetic permeability of free space. Generally, the ionized air produced in the hypersonic flow is a poor electrical conductor, where the induced magnetic field by the plasma current is much smaller than the applied magnetic field and diffuses rapidly. The values of magnetic Reynolds number in this paper are no more than 0.72, which is too small to consider the influence by induced magnetic field [38]. Thus, the induced magnetic field is ignored and the low magnetic field approximation is usually used.

III. Numerical Methods

A. Governing Equations and Calculation Method

Because hypersonic MHD experiments remain largely elusive due to their excessive complexity, numerical simulations were conducted to better understand the unsteady evolutionary process during the movement of the shock wave. The axisymmetric, unsteady, and compressible laminar-flow governing equations are employed, where the coupling computation of the flowfield and the electromagnetic field is accomplished by adding the electromagnetic source term. The present study mainly focuses on bow shock movement process around the sphere, where in particular the boundary layer around the body has no significant influence on the detached distance. Thus, the inviscid flow is calculated and the governing equations are as follows:

$$\frac{\partial \boldsymbol{Q}}{\partial t} + \frac{\partial \boldsymbol{F}}{\partial x} + \frac{\partial \boldsymbol{G}}{\partial r} + \boldsymbol{H} = \boldsymbol{W} + \boldsymbol{S}_M \tag{3}$$

where

$$\boldsymbol{Q} = (\rho_i, \rho u, \rho v, \rho e_t, \rho e_v)^T,$$
$$\boldsymbol{F} = (\rho_i u, \rho u^2 + p, \rho uv, (\rho e_t + p)u, \rho u e_v)^T$$
$$\boldsymbol{G} = (\rho_i, \rho uv, \rho v^2 + p, (\rho e_t + p)v, \rho v e_v)^T$$
$$\boldsymbol{H} = \frac{1}{r}(\rho_i, \rho uv, \rho v^2, (\rho e_t + p)v, \rho v e_v)^T$$
$$\boldsymbol{W} = (\dot{\omega}_i, 0, 0, 0, S_v)^T$$
$$\boldsymbol{S}_M = \left(0, (\boldsymbol{J}\times\boldsymbol{B})_x, (\boldsymbol{J}\times\boldsymbol{B})_r, \boldsymbol{J}\cdot\boldsymbol{E}, \frac{1}{\sigma}\boldsymbol{J}\cdot\boldsymbol{J}\right)^T$$

where x and r are axial and radial coordinates of the physical space, respectively; t is time; $\boldsymbol{Q}$ is the conserved variable vector; $\boldsymbol{F}, \boldsymbol{G}$, and $\boldsymbol{H}$ are inviscid flux vectors; $\boldsymbol{S}_M$ is the electromagnetic source vector; $\boldsymbol{W}$ is the chemical source term. ρ_i represents the density of species i; u and v are axial and radial velocities, respectively; p and ρ are pressure and density, respectively; e_t and e_v are unit mass of total energy and vibrational energy, respectively. $\dot{\omega}_i$ and S_v represent the production rates of mass and vibrational energy.

Additional quantities are required to calculate the electromagnetic source vector $\boldsymbol{S}_M$, and they are electric current density vector $\boldsymbol{J}$, electric strength vector $\boldsymbol{E}$, and magnetic field vector $\boldsymbol{B}$. The generalized Ohm's law is used to solve the current density, and the expression is as follows:

$$\boldsymbol{J} = \sigma(\boldsymbol{E} + \boldsymbol{u}\times\boldsymbol{B}) \tag{4}$$

where σ is the electrical conductivity. Because of the assumption of the axisymmetric two-dimensional electromagnetic field and the neglect of the Hall effect, the electric field $\boldsymbol{E}$ in Eq. (5) becomes zero. Consequently, the electric current density has only the azimuthal θ component, which is written as

$$J_\theta = \sigma(u_x B_r - u_r B_x) \tag{5}$$

Therefore, the electromagnetic source vector is simplified as

$$\boldsymbol{S}_M = \left(0, -J_\theta B_r, J_\theta B_x, 0, \frac{J_\theta^2}{\sigma}\right)^T \tag{6}$$

The seven chemical species are considered in the present study: N, O, N_2, O_2, NO, NO+, and e-. As a finite-rate chemical kinetics model, 18 chemical reactions are included from Refs. [39–42]. Park's two-temperature model is employed to take account of the thermal nonequilibrium state. The vibrational–electron–electronic energy contains the vibrational and electric excitation energies of atoms and molecules. The terms of energy exchange processes include vibrational–translational energy relaxation $Q_{\text{tr-vib}}$, electronic–translational energy relaxation $Q_{\text{tr-el}}$, and vibrational energy loss due to the dissociation $Q_{\text{vib-dis}}$ [27,43].

The expression of the vibration source term S_v is as follows:

$$S_v = Q_{\text{tr-vib}} + Q_{\text{vib-dis}} + Q_{\text{tr-el}}$$
$$Q_{\text{tr-vib}} = \sum_j \frac{\rho_j R_j \theta_{vj}\left(\frac{1}{e^{\theta_{vj}/T_t}-1} - \frac{1}{e^{\theta_{vj}/T_v}-1}\right)}{\tau_{vj}}$$
$$Q_{\text{vib-dis}} = \sum_j w_j \frac{R_j\theta_{vj}}{e^{\theta_{vj}/T_v}-1}$$
$$Q_{\text{tr-el}} = 3\rho_e R(T_t - T_v)\sum_{s\neq e}\frac{\nu_{e,s}}{M_s}$$

where θ_{vj} is the vibrational characteristic temperature of species j; R_j is the gas constant of component j; R is universal gas constant; τ_{vj} is the vibrational relaxation time; M_s is the molecular weight of species S; $\nu_{e,s}$ is the effective collision frequency of electrons with heavy particles.

The governing equations were solved using a finite-difference approach; convective terms were approximated using the AUSMPW+ scheme [44]. Time integration was performed implicitly by applying the LU-SGS algorithm [45]. Noncatalytic isothermal and slip boundary conditions were specified as the boundary conditions at the wall, and the temperature was set to 293 K.

B. Electrical Conductivity Model

The electrical conductivity is required to calculate the current density from the generalized Ohm's law. The commonly used plasma electrical conductivity model is based on the collision theory of molecular motion, which considers the collision and migration process of electrons and ions in plasma. This model not only includes the weak ionization and strong ionization conduction mechanism, but also takes into account the difference of all kinds of gas species. The electrical conductivity is written as [30]

$$\sigma = \frac{n_e e^2}{m_e \sum_{s\neq e}\nu_{e,s}^m} \tag{7}$$

where $\nu_{e,s}^m$ is the effective momentum exchange collision frequency of electrons with other chemical species. When s is the ionic component, the expression is written as

$$\nu_{e,s}^m = 6\pi\left(\frac{e^2}{12\pi\varepsilon_0 k T_e}\right)^2 \ell_n\left[12\pi\left(\frac{\varepsilon_0 k}{e^2}\right)^{3/2}\sqrt{\frac{T_e^3}{n_e^2}}\right] n_s\sqrt{\frac{8kT_e}{\pi m_e}}$$

When s is the neutral particle component, the expression is written as

$$\nu_{e,s}^m = \frac{4}{3}\sigma_{e,s}^m n_s\sqrt{\frac{8kT_e}{\pi m_e}}$$

where k and ε_0 are the Boltzmann constant and vacuum permittivity, respectively; e, m_e, and n_e are the elementary charge, electron mass, and electron number density, respectively; n_s is the number density of the component s; T_e is the electron temperature and is equal to the vibration temperature T_v in the two-temperature model. $\sigma_{e,s}^m$ represents the effective momentum exchange collision cross sections between electrons and other neutral component molecules, and is obtained by using a fitting relation reported in the literature [41].

C. Magnetic Field Model

The dipole magnetic field model, frequently used in experiments [46] and calculations [17], is applied in the present investigation. The origin coordinate is set at the center point of the sphere, and the externally applied magnetic field is assumed to be produced by a dipole magnet placed at the point of $r = 0$ and $x = 0$ inside the sphere. Expression of the magnetic field distribution is as follows:

$$B_r = -\frac{B_0 R_b^3}{2(x^2+r^2)^{3/2}}\frac{3xr}{x^2+r^2} \tag{8}$$

$$B_z = -\frac{B_0 R_b^3}{2(x^2+r^2)^{3/2}}\frac{(2x^2-r^2)}{x^2+r^2} \tag{9}$$

where R_b is the radius of the sphere, and B_0 is the strength of the magnetic flux density at the stagnation point. The present study varies the parameter over a wide range of 0.0–10.0 T for examining influences of the strength of applied magnetic field or magnetic interaction parameter on the formation process of the bow shock. The distribution of the externally applied magnetic field around the sphere for the parameter $B_0 = 5$ T is illustrated in Fig. 3.

D. Grid Independence Study

A grid convergence study was conducted for three different grid resolutions (240×160, 360×240, and 480×320 grid points, with the first numbers representing the grid nodes along the axial

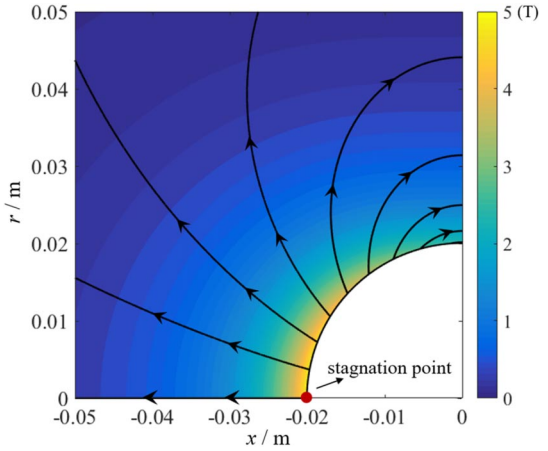

Fig. 3 The distribution of dipole magnetic field around the sphere for $B_0 = 5$ T.

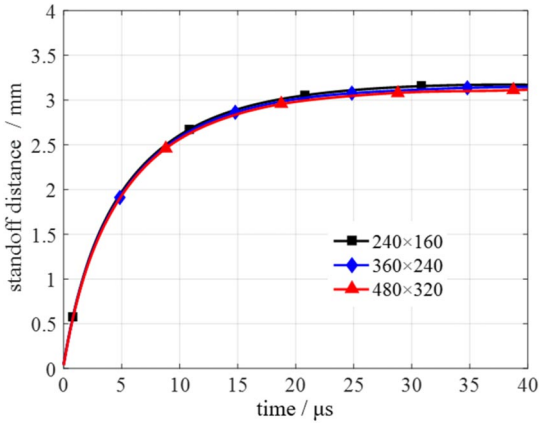

Fig. 4 Shock detached histories for three grid resolutions with $M_s = 13, B_0 = 0$ T, $p_1 = 250$ Pa, $T_1 = 293$ K, and $R_b = 20$ mm.

coordinate; the zones near the wall were incorporated with clustered points). The transient behavior of the shock-detached distance with time was shown in Fig. 4, which showed negligible difference among the three grid resolutions. Thus, a mesh size of 240×160 was employed in the present study considering the computational cost.

IV. Results and Analysis

The diffraction of the incident shock wave over the sphere and the subsequent motion of the reflected shock wave for $M_s = 13$ without an applied magnetic field or with the magnetic field of $B_0 = 8$ T are shown for comparison in Fig. 5. Other parameters are the following: $p_1 = 250$ Pa, $T_1 = 293$ K, and $R_b = 20$ mm. The shock wave moves downstream, strikes the sphere, and is reflected. Initially, this reflection is regular. When the angle of inclination of the incident shock to the surface has increased, Mach reflection occurs. Subsequently, the reflected shock travels upstream before a stable shock wave is established. From the point of wave evolution, the presence of a magnetic field will not produce additional flowfield structure. The present computation is initiated immediately at the shock impingement occurred. The flowfield tends to be stable at the moment of $t = 20$ μs in the absence of magnetic field, whereas when $B_0 = 8$ T, the flow needs 30 μs to become stabilized, and the distance of the detached shock is significantly larger than that in the absence of a magnetic field. The results in Fig. 5 clearly reveal that there are differences in the displacement and velocity of reflected bow shock in the presence or absence of a magnetic field. Figure 6 shows the temperature distribution during formation of bow shock wave for $M_s = 13, B_0 = 0/8$ T, which indicates the similar flowfield in the shock layer between the two cases. Whereas the magnetic field is applied to the plasma flow, an azimuthal electric current J_θ will be

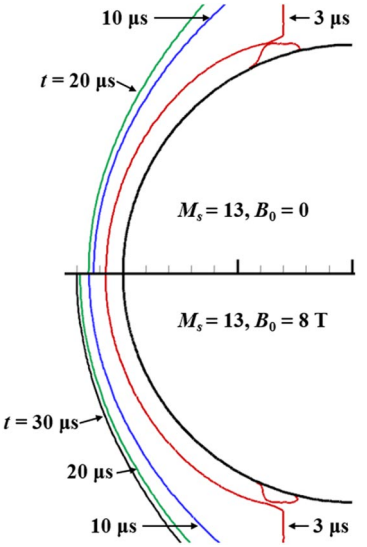

Fig. 5 Transient motion of reflected shock comparison for $M_s = 13, B_0 = 0/8$ T.

induced in the shock layer, as shown in Fig. 2. The interaction between the magnetic field and the azimuthal electric current induces the Lorentz force in the shock layer, as shown in Fig. 7. The Lorentz force decelerates the tangential flow, so that the bow shock wave is pushed away from the sphere by applying the magnetic field.

The displacement–time relationship curves of the reflected shock movement with $M_s = 9$ and $M_s = 13$ are shown in Figs. 8 and 9, respectively. The relationship curves reveal that the higher the incident shock Mach number is, the smaller the shock layer thickness is. This is due to the stronger inertia force of the flow element generated by the higher inflow velocity, which results in a higher degree of gas compression in the shock layer. For the same incident shock Mach number, with the increase of the intensity of the external magnetic field, the stabilization time of the reflected shock is prolonged as a result of the blocking effect of the electromagnetic force generated by the interaction between the magnetic field and the electrically conductive fluid.

When the incident shock Mach number is small, as shown in Fig. 8, as the conductivity is positively correlated with the temperature in the stagnation region, the low incident shock Mach number does not generate sufficient conductivity. As a result, the magnetic interaction parameter under this condition is extremely small, and the interaction between the magnetic field and flowfield can be basically ignored, making it difficult to produce an obvious MHD flow control effect. When the incident shock Mach number is large, as shown in Fig. 9, the high temperature and pressure generated after the reflected shock lead to relatively violent chemical reactions, among which is the ionization process producing a relatively high conductivity. When the magnetic field applied, the tangential flow of the conducting fluid is blocked by Lorentz force, which leads to the increase of the shock-detached distance when it reaches steady. For the process of unsteady formation of the bow shock, the displacement of the reflected shock with a magnetic field is larger than that with a weaker magnetic field at the corresponding moment.

The pressure at the stagnation point can reflect the flow state and the aerodynamic characteristics of the model, which is attracting much attention. Here, the incident shock Mach number of 13 is selected to illustrate the regularity. The time history of the stagnation pressure under such a condition is shown in Fig. 9. At the moment of shock impingement, the stagnation pressure is the maximum in the whole formation process, and it gradually decreases along with time to a steady value. In the presence of a magnetic field, the stagnation pressure decreases more slowly than that with a weaker magnetic field. Whether a magnetic field exists has no effect on the final stable stagnation pressure, that is, the interaction between the magnetic field and the conductive flow only has an effect on the formation process of

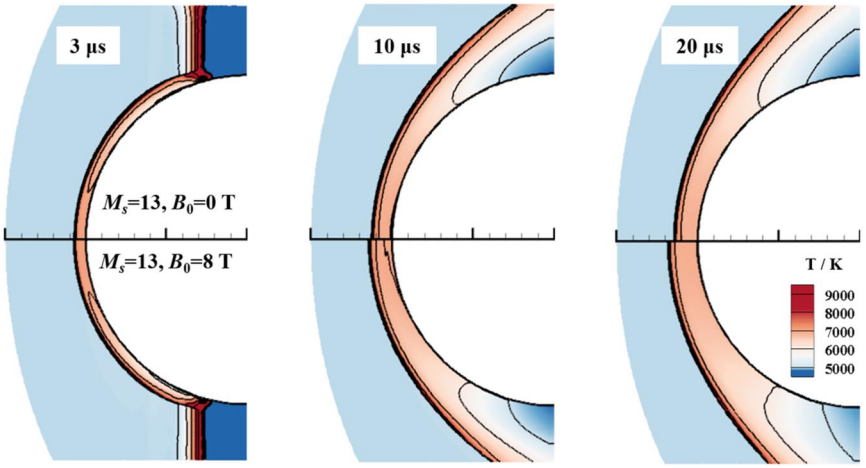

Fig. 6 Temperature distribution during formation of bow shock wave for $M_s = 13, B_0 = 0/8$ T.

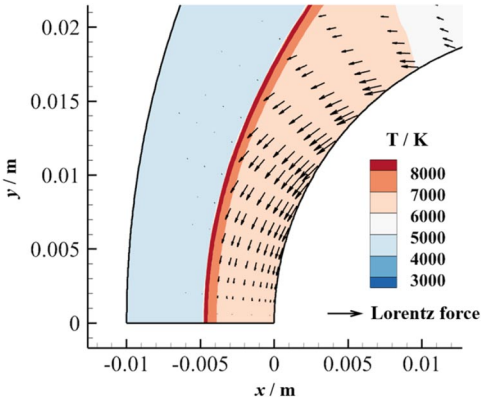

Fig. 7 Two-dimensional distribution of the Lorentz force for $M_s = 13, B_0 = 10$ T, $p_1 = 250$ Pa, $T_1 = 293$ K, and $R_b = 20$ mm.

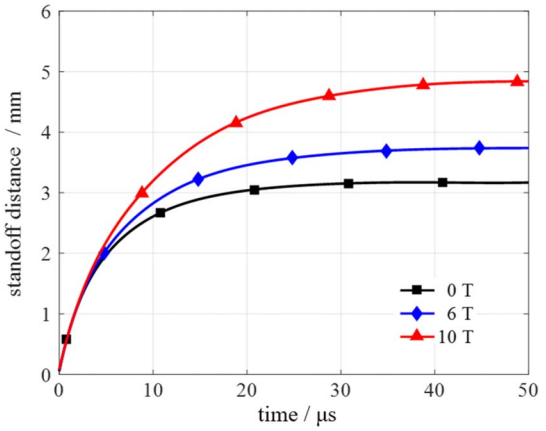

Fig. 9 The displacement–time relationship of the reflected shock with different magnetic field intensities, when the incident shock Mach number $M_s = 13$.

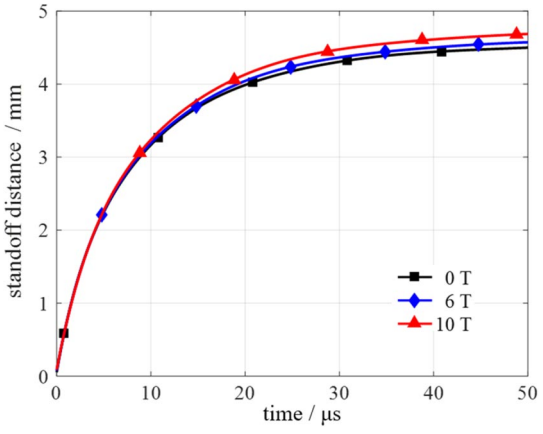

Fig. 8 The displacement–time relationship of the reflected shock with different magnetic field intensities, when the incident shock Mach number $M_s = 9$.

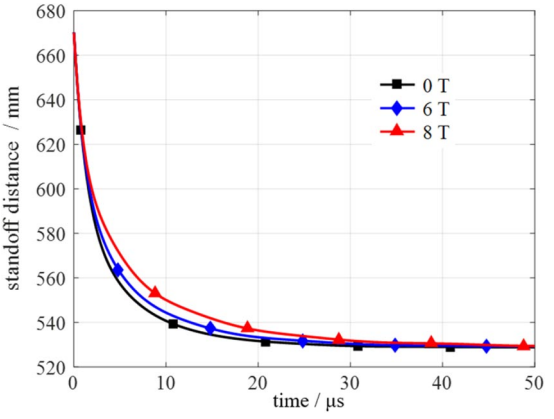

Fig. 10 Time history of the stagnation pressure with different magnetic field intensities.

the stagnation pressure. In other words, the magnetic field can maintain, to some extent, the stagnation pressure at the beginning.

The effect of magnetic field on the time history of the reflected shock displacement and stagnation pressure observed in Figs. 9 and 10 is essentially caused by Lorentz force generated by the interaction between the magnetic field and the conductive flow, of which the direction points to the stagnation line in the shock layer. The force blocks fluid movement along the tangential direction, resulting in a reduced mass outflow rate in the region near the stagnation line after the reflected shock. Therefore, the influence exerted by the magnetic field on the flow parameters near the stagnation line is an important reason to change the formation process of the bow shock. An analysis of the variation regularity of the parameter distribution on the stagnation line with time during the formation of the bow shock is conducted. Comparisons of the temperature and density distribution on the stagnation line at different moments are shown in Figs. 11 and 12, in which the black and red lines respectively represent 0 and 8 T. In the temperature distribution shown in Fig. 11, the curves with or without magnetic field basically coincide at the initial shock reflection stage. With time going on, the temperature at the shock decreases

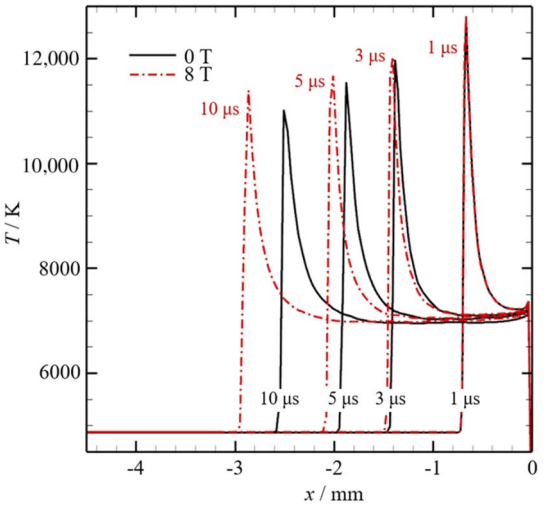

Fig. 11 Comparison of the temperature distribution on the stagnation line with or without magnetic field.

more slowly with magnetic field than without magnetic field, whereas the temperature at the stagnation line behind the shock is almost the same. Regarding the density distribution in Fig. 12, at the initial shock reflection stage, the density distribution curves on stagnation points with or without magnetic fields also basically coincide. With time processing, the postshock density with magnetic field is clearly higher than that without magnetic field at the corresponding time, which directly indicates that the application of the magnetic field enhances the blocking effect on flowing near the stagnation line. Taking together these results, it can be illustrated that the flow state after the reflected shock is higher than that without magnetic field at the corresponding time, and according to the law of shock motion, when the flow parameters in front of the reflected shock are consistent, the higher the flow state behind the shock is, the faster the shock moves. Therefore, the velocity of the reflected shock with the application of the magnetic field is higher at the corresponding time. The preceding analysis shows that a magnetic field is helpful to maintain the velocity of the reflected shock, that is, a weaker velocity attenuation happens when there exists a magnetic field, and thus, the displacement is longer, which helps to acquire a better insight into the phenomenon that the existence of magnetic field leads to the increase of the shock-detached distance from the perspective of the unsteady process.

Because the optical methods will not be significantly affected by the presence of the electromagnetic field, the shock-detached distance/shock structure is one of the most concerned phenomena in hypersonic MHD experiments. The results shown in Figs. 9–11

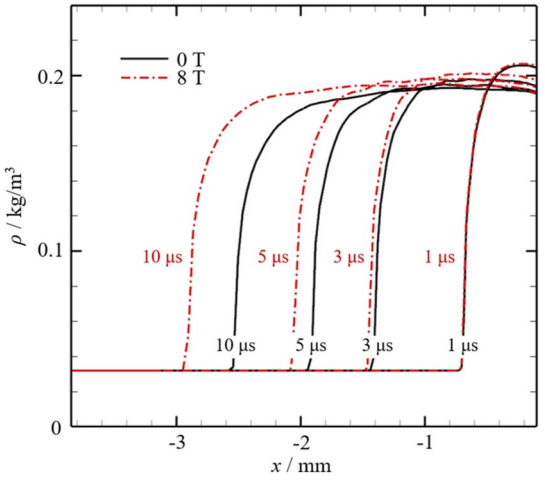

Fig. 12 Comparison of density distribution on the stagnation line with or without magnetic field.

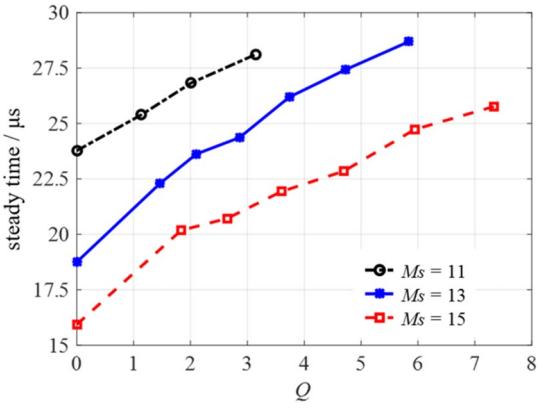

Fig. 13 Diagram of the relationship between stabilization time and the magnetic interaction parameter (dimensional).

reveal that when the magnetic field increases, the time required for the stabilization of the bow shock will also be prolonged. For high-enthalpy impulse equipment, the effective test time is extremely short, thus it becomes necessary to evaluate the unsteady process of the MHD flow experiments to avoid the situation that the steady state is not reached during the test time range. The bow shock formation process considered in this study is highly consistent with the shock tube experimental environment, where the effective test time is on the order of tens of microseconds under the condition of a high-incident-shock Mach number.

The relationship between the stabilization time of the reflected shock and the magnetic interaction parameter is shown in Fig. 13. The stabilization time in this study is defined as the time corresponding to when the reflected shock displacement reaches 95% of the steady detached distance. The results in Fig. 13 show that with the same incident shock Mach number, the time required to reach steady increases as the magnetic interaction parameter gets higher. When magnetic interaction parameter is identical, the higher the incident shock Mach number is, the shorter the stabilization time of the reflected shock needs. Therefore, it could be challenging for MHD experiments under the situation of the high- incident shock Mach number test condition with a large magnetic interaction parameter, or to be more serious, it will happen in certain cases in which the correctness of the results cannot be guaranteed due to the inherent disability of the experiment design, where the flowfield fails in reaching steady.

To further obtain the general regularity, the stabilization time in Fig. 13 is nondimensionalized, as shown in Fig. 14. The reference time used here is the stabilization time of the corresponding incident shock Mach number in the absence of magnetic field, and the abscissa is the magnetic interaction parameter that can reflect the magnetic control effects. From Fig. 14, with the increase of the magnetic

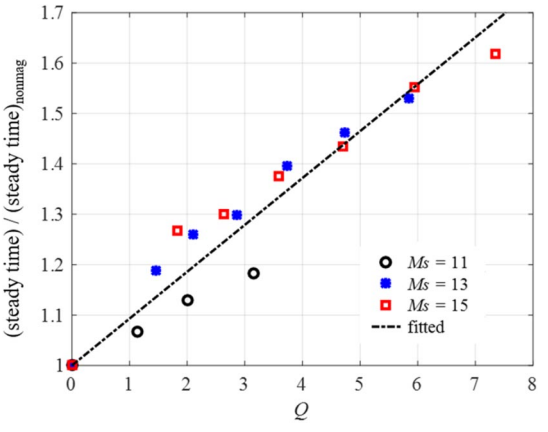

Fig. 14 Diagram of the relationship between the stabilization time and the magnetic interaction parameter (dimensionless).

interaction parameter, the dimensionless time of the bow shock stabilization basically shows a linear increase. In the hypersonic MHD tests, the obvious MHD effects require that Q is larger than 1. In this case, the time needed to establish the stability of the flowfield is increased by about 10%. Meanwhile, the fitting relation of the data in the present paper is also obtained as follows:

$$\frac{t_{\text{steady}}}{t_{\text{steady-nonmag}}} = k_0 \cdot Q + 1$$

where $k_0 = 0.093$. Thus, based on the establishment time of the flowfield in the absence of magnetic field, the characteristic time required for the establishment of bow shock can be quickly evaluated according to the magnetic interaction parameter.

V. Conclusions

The diffraction of an incident shock wave over a sphere under different magnetic field intensities was calculated. The time histories of the reflected shock displacement and the stagnation pressure are presented, which reflects the delay of stabilization when magnetic field was applied. The difference of density distribution along the stagnation line between $B_0 = 0$ and $B_0 = 8$ T under $M_s = 13$ demonstrates a blocking effect caused by Lorentz force. The time needed to establish the steady flows is displaced against the magnetic interaction parameter. The results show that the larger the magnetic interaction parameter is, the longer the establishment time a steady bow shock needs. Further, linear fitting is conducted for the calculated points to reflect the regularity, and the linear relationship shows that the stabilization time could increases 46.7% when $Q = 5$, which challenges the impulsive facilities to have sufficient test times for conducting MHD experiments. This study could provide guidance for the design of hypersonic MHD experiments in shock tubes or expansion tubes.

Acknowledgments

This work was supported by the National Natural Science Foundation of China (grant nos. 12072352)

References

[1] Berger, K., Anderson, B., Campbell, C., Garske, M., Saucedo, L., Kinder, G., and Micklos, A., "Boundary Layer Transition Flight Experiment Overview," AIAA Paper 2011-3323, June 2011. https://doi.org/10.2514/6.2011-3323

[2] Zhu, W., Shi, M., Zhu, Y., and Lee, C., "Experimental Study of Hypersonic Boundary Layer Transition on a Permeable Wall of a Flared Cone," *Physics of Fluids*, Vol. 32, Jan. 2020, Paper 011701. https://doi.org/10.1063/1.5139546

[3] Zhu, W., Chen, X., Zhu, Y., and Lee, C., "Nonlinear Interactions in the Hypersonic Boundary Layer on the Permeable Wall," *Physics of Fluids*, Vol. 32, Oct. 2020, Paper 104110. https://doi.org/10.1063/5.0028698

[4] Mehta, R., "Numerical Simulation of Self-Sustained Oscillations over Spiked Blunt-Bodies," AIAA Paper 2001-0262, Jan. 2001. https://doi.org/10.2514/6.2001-262

[5] Sun, X. W., Guo, Z. Y., Huang, W., Li, S. B., and Yan, L., "A Study of Performance Parameters on Drag and Heat Flux Reduction Efficiency of Combinational Novel Cavity and Opposing Jet Concept in Hypersonic Flows," *Acta Astronautica*, Vol. 131, Feb. 2017, pp. 204–225. https://doi.org/10.1016/j.actaastro.2016.11.044

[6] Kim, M., "Active Plasma Layer Manipulation Scheme During Hypersonic Flight," *Aerospace Science and Technology*, Vol. 35, March 2014, pp. 135–142. https://doi.org/10.1016/j.ast.2014.03.008

[7] Kim, M., Keidar, M., and Boyd, I. D., "Analysis of an Electromagnetic Mitigation Scheme for Reentry Telemetry Through Plasma," *Journal of Spacecraft and Rockets*, Vol. 45, No. 6, 2008, pp. 1223–1229. https://doi.org/10.2514/1.37395

[8] Kim, M., "Electromagnetic Manipulation of the Plasma Layer for Re-Entry Blackout Mitigation," Ph.D. Thesis, Dept. of Aerospace Engineering, Univ. of Michigan, Ann Arbor, MI, 2009.

[9] Li, Y. W., Zhang, B. L., Li, Y. H., Xiao, L. H., Wang, Y. T., and He, G. Q., "Applications and Prospects of Magneto-Hydrodynamics in Aeronautical Engineering," *Advances in Mechanics*, Vol. 47, No. 1, 2017, pp. 452–502. https://doi.org/10.6052/1000-0992-16-036

[10] Otsu, H., Matsuda, A., Abe, T., and Konigorski, D., "Feasibility Study on the Flight Demonstration for a Reentry Vehicle with the Magnetic Flow Control System," AIAA Paper 2006-3566, June 2006. https://doi.org/10.2514/6.2006-3566

[11] Girgis, I., Shneider, M. N., Macheret, S., Brown, G., and Miles, R. B., "Steering Moments Creation in Supersonic Flow by Off-Axis Plasma Heat Addition," *Journal of Spacecraft and Rockets*, Vol. 43, No. 3, 2006, pp. 607–613. https://doi.org/10.2514/1.16708

[12] Gnemmi, P., Charon, R., Dupéroux, J. P., and George, A., "Feasibility Study for Steering a Supersonic Projectile by a Plasma Actuator," *AIAA Journal*, Vol. 46, No. 6, 2008, pp. 1308–1317. https://doi.org/10.2514/1.24696

[13] Kakutani, T., "Axially Symmetric Stagnation-Point Flow of an Electrically Conducting Fluid Under Transverse Magnetic Field," *Journal of the Physical Society of Japan*, Vol. 15, No. 4, 1960, pp. 688–695. https://doi.org/10.1143/JPSJ.15.688

[14] Rossow, V. J., "On Flow of Electrically Conducting Fluids over a Flat Plate in the Presence of a Transverse Magnetic Field," NACA TR-1358, 1958.

[15] Romig, M. F., "The Influence of Electric and Magnetic Fields on Heat Transfer to Electrically Conducting Fluids," *Advances in Heat Transfer*, edited by T. F. Irvine, and J. P. Hartnett, Vol. 1, Elsiever, New York, 1964, pp. 267–354. https://doi.org/10.1016/S0065-2717(08)70100-X

[16] Ludford, G. S. S., and Murray, J. D., "On the Flow of a Conducting Fluid Past a Aagnetized Sphere," *Journal of Fluid Mechanics*, Vol. 7, No. 4, 1960, pp. 516–528. https://doi.org/10.1017/S0022112060000268

[17] Bush, W. B., "Magnetohydrodynamic-Hypersonic Flow Past a Blunt Body," *Journal of the Aerospace Sciences*, Vol. 25, No. 11, 1958, pp. 685–690. https://doi.org/10.2514/8.7845

[18] Li, Y. X., Wang, Q., Luo, K., Li, J. P., and Zhao, W., "Theoretical Analysis on Hypersonic MHD Shock Stand-Off Distance of Blunt Body," *Chinese Journal of Theoretical and Applied Mechanics*, Vol. 53, No. 9, 2021, pp. 2493–2500. https://doi.org/10.6052/0459-1879-21-127

[19] Lykoudis, P. S., "The Matching of the Viscid and Inviscid Regions for the Stagnation Magnetic Flow," *Journal of the Aerospace Sciences*, Vol. 26, No. 5, 1959, pp. 315–317. https://doi.org/10.2514/8.8060

[20] Ziemer, R. W., and Bush, W. B., "Magnetic Field Effects on Bow Shock Stand-Off Distance," *Physical Review Letters*, Vol. 1, No. 2, 1958, pp. 58–59. https://doi.org/10.1103/PhysRevLett.1.58

[21] Cambel, A. B., Yuen, M. C., Porter, R., Nowak, R., Kranc, S., and Chang, C., "Theoretical and Experimental Studies of Magneto-Aerodynamic Drag and Shock Standoff Distance," NASA CR-70315, 1966.

[22] Kawamura, M., Nagata, Y., Katsurayama, H., Otsu, H., Yamada, K., and Abe, T., "Magnetoaerodynamic Force on a Magnetized Body in a Partially Ionized Flow," *Journal of Spacecraft and Rockets*, Vol. 50, No. 2, 2013, pp. 347–351. https://doi.org/10.2514/1.A32279

[23] Gildfind, D. E., Smith, D., Lefevre, A., Jacobs, P. A., and McIntyre, T. J., "Magnetohydrodynamic Aerobraking Shock Stand-Off Measurements with Flight Representative Electrodynamic Boundary Conditions," *AIAA Journal*, Vol. 60, No. 1, Oct. 2021, pp. 41–55. https://doi.org/10.2514/1.J060466

[24] Lineberry, J., Begg, L., Castro, J., Litchford, R., and Donohue, J., "HVEPS Scramjet-Driven MHD Power Demonstration Test Results," AIAA Paper 2007-3880, June 2007. https://doi.org/10.2514/6.2007-3880

[25] Lapushkina, T. A., and Erofeev, A. V., "Supersonic Flow Control via Plasma, Electric and Magnetic Impacts," *Aerospace Science and Technology*, Vol. 69, Oct. 2017, pp. 313–320. https://doi.org/10.1016/j.ast.2017.06.033

[26] Palmer, G., "Magnetic Field Effects on the Computed Flow over a Mars Return Aerobrake," *Journal of Thermophysics and Heat Transfer*, Vol. 7, No. 2, 1993, pp. 294–301. https://doi.org/10.2514/3.419

[27] Fujino, T., and Ishikawa, M., "Numerical Simulation of Control of Plasma Flow with Magnetic Field for Thermal Protection in Earth Reentry Flight," *IEEE Transactions on Plasma Science*, Vol. 34, No. 2, 2006, pp. 409–420. https://doi.org/10.1109/TPS.2006.872458

[28] Shimosawa, Y., and Fujino, T., "Numerical Study of Magnetohydrodynamic Flow Control Along Superorbital Reentry Trajectories," *Journal of Spacecraft and Rockets*, Vol. 53, No. 3, 2016, pp. 528–537. https://doi.org/10.2514/1.A33340

[29] Gu, S., and Olivier, H., "Capabilities and Limitations of Existing Hypersonic Facilities," *Progress in Aerospace Sciences*, Vol. 113, Feb. 2020, Paper 100607. https://doi.org/10.1016/j.paerosci.2020.100607

[30] Ding, M. S., Jiang, T., Liu, Q. Z., Dong, W. Z., Gao, T. S., and Fu, Y. A. X., "Impact of Simulation of Electrical Conductivity on Hypersonic MHD Control," *Acta Aeronauticaet Astronautica Sinica*, Vol. 40, No. 11, 2019, p. 23009. https://doi.org/10.7527/S1000-6893.2019.23009

[31] Xiong, Z., Zhang, Y. Y., Wang, S., Li, J. P., Chen, H., Fan, B. C., and Cui, J. P., "An Improved Experiment for Electromagnetic Wave Transmission in Shock Tube," *Chinese Journal of Theoretical and Applied Mechanics*, Vol. 50, No. 6, 2018, pp. 1328–1336. https://doi.org/10.6052/0459-1879-18-284

[32] Lefevre, A., Gildfind, D. E., Gollan, R. J., Wei, H., and McIntyre, T., "Expansion Tube Experiments of Magneto- Hydrodynamic Aerobraking for Superorbital Earth Reentry," *AIAA Journal*, Vol. 59, No. 8, 2021, pp. 3228–3240. https://doi.org/10.2514/1.J060253

[33] Patz, G., "Formation of Bow Waves Around Blunt Bodies in the Flow Behind a Moving Shock," *Acta Mechanica*, Vol. 32, No. 1, 1979, pp. 89–100. https://doi.org/10.1007/BF01176136

[34] Moran, J. P., and Moorhem, W. K. V., "Diffraction of a Plane Shock by an Analytic Blunt Body," *Journal of Fluid Mechanics*, Vol. 38, No. 1, 1969, pp. 127–136. https://doi.org/10.1017/S0022112069000085

[35] Barnwell, R. W., "Numerical Results for the Diffraction of a Normal Shock Wave by a Sphere and for the Subsequent Transient Flow," NASA TR-R-268, 1967.

[36] Miller, C. G., and Moore, J. A., "Flow-Establishment Times for Blunt Bodies in an Expansion Tube," *AIAA Journal*, Vol. 13, No. 12, 1975, pp. 1676–1678. https://doi.org/10.2514/3.7048

[37] Nagata, Y., Satofukay, Y., Watanabey, Y., Tezukaz, A., Yamadax, K., and Abe, T., "Experimental Study on the Magneto-Aerodynamic Force Deflected by Magnetic Field Interaction in a Weakly-Ionized Plasma Flow," AIAA Paper 2013-2999, Jan. 2015.

[38] Poggie, J., and Gaitonde, D., "Computational Studies of Magnetic Control in Hypersonic Flow," AIAA Paper 2001-0196, Jan. 2001. https://doi.org/10.2514/6.2001-196

[39] Dunn, M. G., and Kang, S., "Theoretical and Experimental Studies of Reentry Plasmas," NASA CR-2232, 1973.

[40] Blottner, F. G., Johnson, M., and Ellis, M., "Chemically Reacting Viscous Flow Program for Multi-Component Gas Mixtures," Sandia Labs. TR SC-RR-70-754, 1971. https://doi.org/10.2172/4658539

[41] Gnoffo, P. A., "Conservation Equations and Physical Models for Hypersonic Air Flows in Thermal and Chemical Nonequilibrium," NASA TP-2867, 1989.

[42] Gupta, R. N., Yos, J. M., Thompson, R. A., and Lee, K. P., "A Review of Reaction Rates and Thermodynamic and Transport Properties for an 11-Species Air Model for Chemical and Thermal Nonequilibrium Calculations to 30000 K," NASA RP-1232, 1990.

[43] Furumoto, G. H., Zhong, X., and Skiba, J. C., "Numerical Studies of Real-Gas Effects on Two-Dimensional Hypersonic Shock-Wave/Boundary-Layer Interaction," *Physics of Fluids*, Vol. 9, No. 1, 1997, pp. 191–210. https://doi.org/10.1063/1.869162

[44] Kim, K. H., Kim, C., and Rho, O. H., "Methods for the Accurate Computations of Hypersonic Flows: I. AUSMPW+ Scheme," *Journal of Computational Physics*, Vol. 174, No. 1, 2001, pp. 38–80. https://doi.org/10.1006/jcph.2001.6873

[45] Jameson, A., and Yoon, S., "Lower-Upper Implicit Schemes with Multiple Grids for the Euler Equations," *AIAA Journal*, Vol. 25, No. 7, 1987, pp. 929–935. https://doi.org/10.2514/3.9724

[46] Smith, D. R., Gildfind, D. E., Jacobs, P. A., Cullen, T. G., James, C. M., Liu, Y., and McIntyre, T. J., "Magneto-Hydrodynamic Drag Measurements in an Expansion Tunnel with Argon Test Gas," *AIAA Journal*, Vol. 58, No. 10, 2020, pp. 4495–4504. https://doi.org/10.2514/1.J059540

R. M. Cummings
Associate Editor